

3D Porous Garnet/Gel Polymer Hybrid Electrolyte for Safe Solid-State Li–O₂ Batteries with Long Lifetimes

Changtai Zhao, Qian Sun, Jing Luo, Jianneng Liang, Yulong Liu, Lei Zhang, Jiwei Wang, Sixu Deng, Xiaoting Lin, Xiaofei Yang, Huan Huang, Shangqian Zhao, Li Zhang, Shigang Lu, and Xueliang Sun*



Cite This: *Chem. Mater.* 2020, 32, 10113–10119



Read Online

ACCESS |



Metrics & More

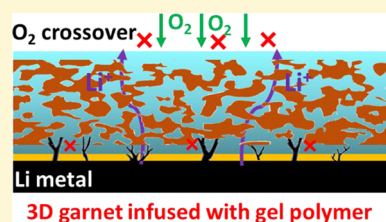


Article Recommendations



Supporting Information

ABSTRACT: Li–O₂ battery is a promising rechargeable battery candidate due to its ultrahigh theoretical energy density. However, safety issues and poor cycling stability of Li–O₂ batteries caused by the formation of Li dendrites and the use of organic liquid electrolytes inhibit their practical applications. Here, we propose a hybrid solid electrolyte composed of three-dimensional (3D) porous garnet microstructure (PSSE) infused with gel polymer electrolyte (GPE) (PSSE/GPE) to enhance the safety and cycling stability of Li–O₂ batteries. In this hybrid solid electrolyte, the 3D garnet microstructure serves as a rigid backbone to suppress Li dendrites, while the consecutive GPE in PSSE serves as an ionic highway, ensuring a high ionic conductivity ($1.06 \times 10^{-3} \text{ S cm}^{-1}$) in the bulk. Besides, the hybrid electrolyte offers the ability to block O₂ crossover and maintain good compatibility with Li metal anode and advanced air electrode. As a result, the cycle life of Li symmetric cell is dramatically improved almost 60 times (6000 h, 250 days) by replacing GPE with PSSE/GPE. The Li–O₂ battery based on PSSE/GPE shows a long cycle life of 194 cycles with a high cycling capacity of 1250 mA h g⁻¹. The present study demonstrates a novel class of hybrid solid electrolyte for high-performance solid-state Li–O₂ batteries.



INTRODUCTION

Safe and high-energy-density rechargeable batteries are highly desired for meeting the ever-increasing demand for energy storage.^{1–3} Li–O₂ batteries featuring the highest theoretical energy density of 3500 W h kg⁻¹ have attracted considerable attention.^{4–7} However, the safety issues and poor cycling stability of Li–O₂ batteries, caused by the Li dendrite growth and the use of organic liquid electrolyte (LEs), inhibit their practical applications.^{8–11} The undesired formation of Li dendrites on the Li metal anode surface and continuous side reactions between dendritic Li and LEs can result in low Coulombic efficiency and poor cycling stability.^{12–15} Additionally, accumulated Li dendrites can penetrate the separator and short-circuit the cell, leading to hazards of thermal runaway and explosion accidents.^{16–19} In an open system of Li–O₂ batteries, the use of LEs even causes additional issues such as solvent evaporation, leakage, and flammability.^{20–23} To address these issues and construct safer Li–O₂ batteries, replacing the organic LEs with solid-state electrolytes (SSEs) is regarded as an ideal approach to solving safety concerns of Li metal anodes, meanwhile avoiding the evaporation, leakage, and flammability of organic LEs.^{24–27}

Among SSE candidates, polymer-based SSEs feature the advantages of processability and flexibility for wearable electronics, but the low ionic conductivity at room temperature alternatively requires operation at an elevated temperature. Unfortunately, the elevated operating temperature will aggravate the side reactions between polymer and discharge products of Li–O₂ batteries.^{28–30} Although sulfide SSEs have

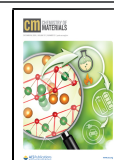
comparable ionic conductivity to LEs, the poor stabilities against Li metal and in air severely limit their feasibility in Li–O₂ batteries and not to mention Li–air batteries.³¹ Oxide SSEs can be one of the most promising SSEs for solid Li–O₂ batteries because of their high electrochemical stability, good chemical stability in air, and excellent mechanical strength.^{12,32–34} Oxide SSEs are also attractive for their high shear modulus that afford the exceptional capability to suppress Li dendrites and eliminate consequent short circuits.^{35–37} Particularly, the garnet-type oxide SSEs possess good stability against Li metal.^{38,39} But the relatively low ionic conductivity and large interfacial resistance between SSEs and electrodes often lead to severe polarization of batteries.^{40,41} These drawbacks can be even worse for Li–O₂ batteries, which intrinsically feature sluggish electrochemical dynamics due to the unique triphase reaction.^{42–44} Therefore, simultaneously achieving high ionic conductivity and good interfacial contact with electrodes is key to build oxide SSE-based Li–O₂ batteries.^{45,46}

Herein, a hybrid solid electrolyte consisting of three-dimensional (3D) porous garnet microstructure (PSSE) with infused gel polymer electrolyte (GPE) (PSSE/GPE) is

Received: September 1, 2020

Revised: November 5, 2020

Published: November 17, 2020



proposed for Li–O₂ batteries. The Li metal symmetric cell using this hybrid electrolyte exhibited excellent cycling stability, with almost 60 times longer plating/stripping duration than using pure GPE. In addition, Li–O₂ batteries based on this hybrid electrolyte showed a long cycle life of 194 cycles with a high limited capacity of 1250 mA h g⁻¹, corresponding to an operating duration of over 1500 h. The outstanding electrochemical performance is attributed to the unique structure of 3D garnet microstructure hybridizing with GPE, which can suppress Li dendrites, enable good interfacial contact, and have high ionic conductivity.

RESULTS AND DISCUSSION

The synthesis process of the hybrid electrolyte is schematically illustrated in Figure 1. First, the Li_{6.4}La₃Zr_{1.4}Ta_{0.6}O₁₂

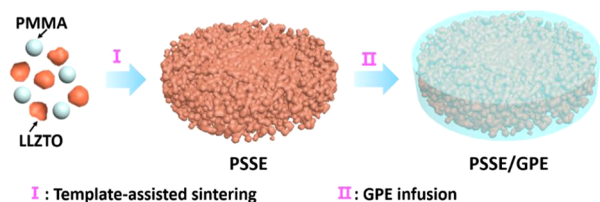


Figure 1. Schematic illustration for the synthesis of PSSE/GPE.

(LLZTO)-based porous SSE (PSSE) was prepared by a template-assisted sintering method, where poly(methyl methacrylate) (PMMA) nanospheres were used as the templates for creating pores. Subsequently, a homogeneous solution of tetraethylene glycol dimethyl ether (TEGDME), LiClO₄ salt, poly(vinylidene fluoride-*co*-hexafluoropropylene) (PVDF-HFP), and acetone was infused into the PSSE framework. After drying, the PSSE/GPE hybrid electrolyte was obtained. To be fair, a dense solid-state electrolyte (DSSE) following the traditional sintering method and a pure GPE by solution casting were also prepared for comparison. As shown in Figure S1, the as-prepared GPE is free-standing and flexible.

The morphology and structure of the as-prepared PSSE and hybrid PSSE/GPE were investigated by scanning electron microscopy (SEM). As shown in Figure 2a–c, the as-prepared PSSE featured interconnected porous structure, with pore sizes ranging from 10 to 100 μm. The high-magnification SEM image shows that the framework was constructed with uniform LLZTO particles (ca. 5 μm, Figure S2). In addition to the micron-sized pores, nanosized pores close to the particle size of

PMMA template (300 nm, Figure S3) were present in the framework, forming a hierarchically porous structure in the PSSE. This further improved the continuity of interconnected channels in PSSE. The high porosity of 69.2% of the PSSE enabled a high filling proportion of GPE with good continuity. As shown in Figures 2d,e and S4, most of the micro- and nanopores of PSSE were filled with GPE after infusion. The filling can potentially block O₂ crossover for Li–O₂ batteries. The high-magnification SEM image shows that the PSSE framework maintained intimate contact with the GPE, ensuring fast Li-ion transport between PSSE and GPE. Li-ion transport through the whole matrix of the hybrid electrolyte, not limited to either PSSE or GPE phase, becomes possible, which is beneficial to high ionic conductivity. As shown in Figure 2f, the consecutive GPE featuring high ionic conductivity serves as “sailing paths” for rapid and massive Li-ion transportation, while the PSSE framework featuring a moderate ionic conductivity offers “hiking paths” for additional Li-ion supply to complete the sophisticated paths for Li-ion transport and ultimately high ionic conductivity. The ionic conductivity of the PSSE/GPE hybrid electrolyte was tested as shown in Figures S5 and S6. It is determined as 1.06 × 10⁻³ S cm⁻¹, which is comparable to that of the pure GPE (3.48 × 10⁻³ S cm⁻¹) and 4 times higher than that of pure DSSE electrolyte (2.0 × 10⁻⁴ S cm⁻¹). The critical current density of PSSE/GPE was tested with a limited capacity of 0.2 mA h cm⁻². As shown in Figure S7, the voltage profiles of Li symmetric battery with PSSE/GPE keep good shapes before the current density increase up to 1.6 mA cm⁻². When the current density increases to 1.6 mA cm⁻², the voltage increases sharply. And the voltage exceeds the limit at the current density of 3.2 mA cm⁻².

The electrochemical properties of the PSSE/GPE hybrid electrolyte were investigated by electrochemical impedance spectroscopy (EIS) and galvanostatic discharge/charge tests. As shown in Figure 3a, the Li metal symmetric cell with PSSE/GPE showed a similar charge transfer resistance to the cell with pure GPE, which suggests that flooded GPE layers on the outer surface PSSE/GPE effectively ensured good interfacial contact (Figure S4). The long-term cycling stability of the Li metal symmetric cells was tested with a limited capacity of 0.2 mA h cm⁻² at a current density of 0.1 mA cm⁻². As shown in Figure 3b, the cell with pure GPE exhibited an obvious increase in overpotential upon cycling and soon short-circuited in 100 h. In sharp contrast, the cell with PSSE/GPE showed

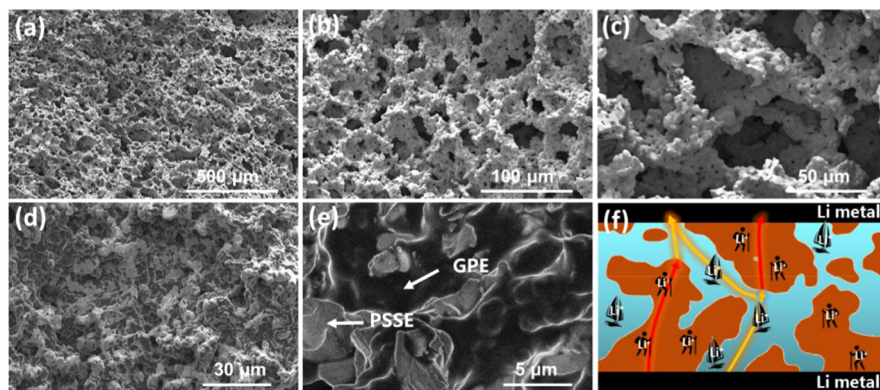


Figure 2. (a–c) SEM images of the as-prepared PSSE. (d, e) SEM images of the as-prepared PSSE/GPE. (f) Schematic illustration for the Li-ion transportation in PSSE/GPE.

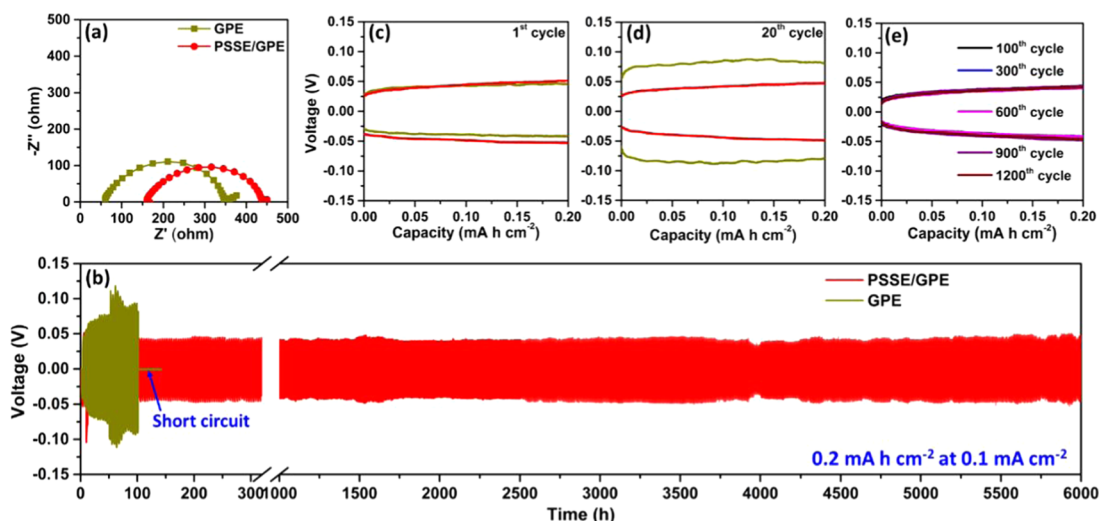


Figure 3. (a) Nyquist plots of the Li metal symmetric cells with GPE and PSSE/GPE, respectively. (b) Cycling stability of Li metal symmetric cell with GPE and PSSE/GPE, respectively, with a limited capacity of 0.2 mA h cm^{-2} at a current density of 0.1 mA cm^{-2} . The corresponding discharge/charge profiles at the (c) 1st cycle and (d) 20th cycle. (e) Discharge/charge profiles at the 100th, 300th, 600th, 900th, and 1200th cycles of the PSSE/GPE cell.

excellent cycling stability over 6000 h. In other words, the cycle life of Li symmetric cell is dramatically improved almost 60 times by replacing the GPE with this hybrid electrolyte. Taking a closer look into discharge/charge profiles, the GPE and PSSE/GPE cells exhibited similar overpotentials in the first cycle, confirming the high ionic conductivity and low interfacial resistance of PSSE/GPE (Figure 3c). While the overpotential of the GPE cell obviously enlarged and became fluctuating at the 20th cycle (Figure 3d), the PSSE/GPE cell maintained highly stable profiles over 1200 cycles, demonstrating excellent cycling stability. (Figures 3d,e, and S8). To further confirm the stability of Li metal symmetric cell with PSSE/GPE, the EIS test was conducted during the cycling process. As shown in Figure S9, the EIS impedances of cell at different cycles kept stable, and the voltage profiles were matched with voltage values calculated by multiplying the EIS impedance and current (0.0712 mA , current density: 0.1 mA cm^{-2} , area: 0.712 cm^{-2}), indicating good stability. The Li metal surface after cycling was investigated by SEM. As shown in Figure S10a–c, after cycling for 25 cycles, the Li metal anode with PSSE/GPE electrolyte showed a relatively flat surface without exfoliated particles. In sharp contrast, Figure S10d–f shows a lot of large particles on the surface of Li metal with GPE electrolyte. These were dead Li formed during cycling. The accumulation of dead Li on Li metal anode surface with GPE caused the polarization of battery, which is consistent with the electrochemical performance of Li metal symmetric cell.

To further highlight the rationalities and advantages of the PSSE/GPE design, electrolytes consisting of either pure DSSE or DSSE/GPE hybrid electrolyte were prepared and compared. As shown in Figure S11, the DSSE features a dense structure. As shown in Figure S12, the Li metal symmetric cell with DSSE showed a huge charge transfer resistance due to the bad interfacial contact.⁴⁷ By modifying the DSSE surface with GPE, significant interfacial contact enhancement was demonstrated by the obvious decrease in charge transfer resistance. Unfortunately, the Li metal symmetric cell with DSSE/GPE still encountered a short circuit after 320 h of cycling (Figure S13). The occurrence of short circuits with DSSE may be

attributed to the formation of Li dendrites along the grain boundary of LLZTO particles, which may be caused by its high electronic conductivity.⁴⁸ Compared with DSSE, the infused GPE in PSSE/GPE features low electronic conductivity that can effectively avoid the combination between Li ions and electrons at the grain boundary of LLZTO. Compared with GPE, 3D porous garnet microstructure in PSSE/GPE features great mechanical properties so that it can serve as a rigid backbone to suppress Li dendrites. Based on the advantages of high ionic conductivity, low interfacial resistance, and effective Li dendrite suppression, the hybrid electrolyte of PSSE/GPE is promising for safe and long-life Li–O₂ batteries.

For constructing a high-performance Li–O₂ battery, the compatibility of the designed PSSE/GPE with an advanced air electrode needs to be evaluated. In this study, a composite film of carbon nanotubes (CNTs) and Mn₃O₄ nanowires with RuO₂ nanoparticles was fabricated as an efficient air electrode featuring high porosity, high conductivity, and excellent catalytic activity.⁴⁹ As shown in Figure 4, the Mn₃O₄ nanowires served as the mechanical framework to support the porous structure; CNTs twined in the framework as electronic

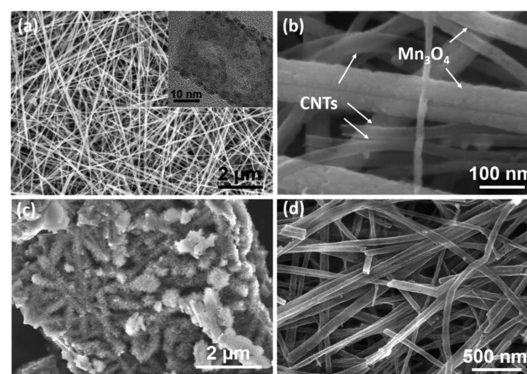


Figure 4. (a, b) SEM images of the as-made CNT/Mn₃O₄–RuO₂ air electrode; the inset is the transmission electron microscopy (TEM) image of CNT/Mn₃O₄–RuO₂ air electrode. SEM images of the air electrode after (c) full discharge and (d) recharge.

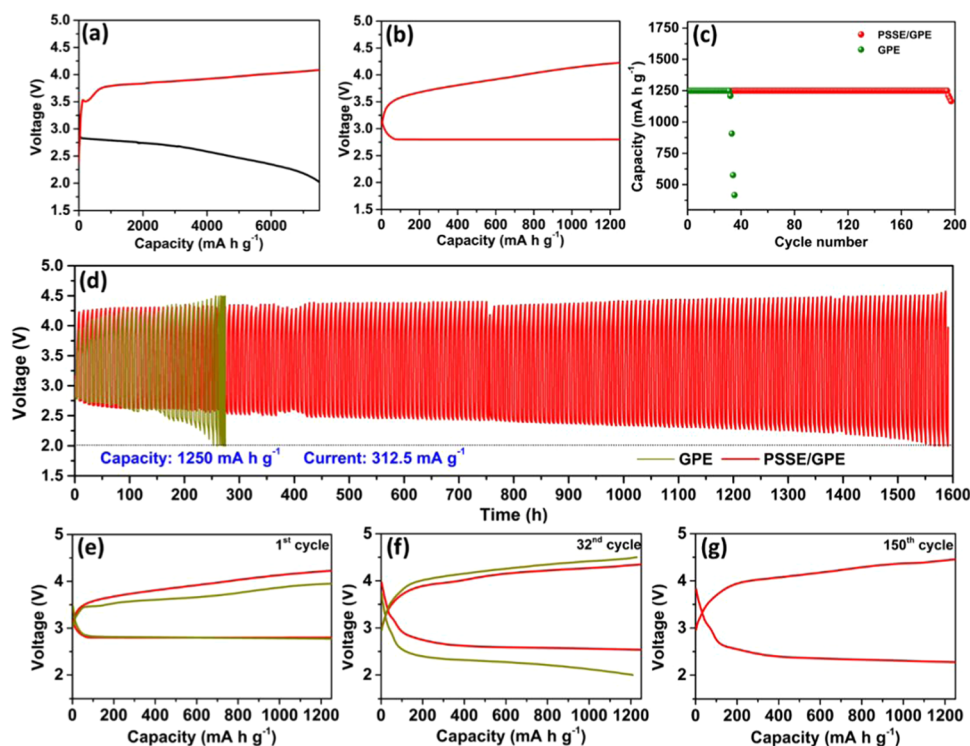


Figure 5. (a) Initial discharge/charge curves of Li–O₂ battery with PSSE/GPE at a current density of 312.5 mA g^{−1}. (b) Discharge/charge curves of a PSSE/GPE-based Li–O₂ battery with a capacity of 1250 mA h g^{−1} at a current density of 312.5 mA g^{−1}. (c) Cycling stability of Li–O₂ batteries with GPE and PSSE/GPE, respectively, with a limited capacity of 1250 mA h g^{−1} at a current density of 312.5 mA g^{−1}. (d) The corresponding discharge/charge profiles during the cycling performance test. The discharge/charge profiles of Li–O₂ batteries with GPE and PSSE/GPE at the (e) 1st cycle, (f) 32nd cycle, and (g) 150th cycle.

conductors for fast electron transfer, and RuO₂ nanoparticles were deposited uniformly on the composite film by atomic layer deposition (ALD) as high-efficiency catalysts for accelerating the decomposition of the discharge product. The energy-dispersive X-ray spectroscopy (EDX) elemental mappings shown in Figure S14 confirmed the uniform distribution of CNTs, Mn₃O₄ nanowires, and RuO₂ nanoparticles in the composite air electrode. The particle size of RuO₂ is about 2 nm.

Li–O₂ batteries using the efficient composite air electrode and the proposed PSSE/GPE were evaluated by galvanostatic discharge/charge cycling tests. As shown in Figure 5a, the Li–O₂ battery delivered a high initial discharge specific capacity of 7540 mA h g^{−1} at a current density of 312.5 mA g^{−1}. Subsequently, the battery can be fully charged to the capacity. As shown in Figure 4c, after discharging, the air electrode was completely covered by the discharge products. After charging, the discharge products disappeared, recovering the original structure of the air electrode (Figure 4d). The excellent catalytic capacity of the advanced air electrode and compatibility with the PSSE/GPE were demonstrated. With a limited capacity of 1250 mA h g^{−1} at a current density of 312.5 mA g^{−1}, the Li–O₂ battery exhibited a stable and low overpotential (Figure 5b). The cycling stability was tested with this high capacity of 1250 mA h g^{−1} per cycle at a current density of 312.5 mA g^{−1} (Figure 5c). The Li–O₂ battery with PSSE/GPE showed a long cycling life up to 194 cycles without capacity decay. The Li–O₂ battery with pure GPE only sustained for 31 cycles. The corresponding discharge/charge profiles also confirmed the stable cycling performance and long cycle life of more than 1500 h for the Li–O₂ battery with

PPSE/GPE (Figure 5d–g). Comparing the electrochemical performance of this work with the work previously reported in the literature (Table S1), it is noted that the performance of the battery in this work was comparable to the best performance of the Li–O₂ batteries with hybrid solid-state electrolytes. These encouraging results proved the versatile advantages of PSSE/GPE as an electrolyte for solid-state Li metal batteries, especially Li–O₂ battery, in terms of the high ionic conductivity, good interfacial contact, and effective suppression for Li dendrites.

The comprehensive effects of the PSSE/GPE hybrid electrolyte, pure GPE, LE, and DSSE in Li–O₂ batteries are schematically compared in Figure 6. The effects are generally in terms of Li-ion conductivity, interfacial contact, O₂ crossover prevention, and Li dendrite suppression. It should be noted that, in the PSSE/GPE hybrid electrolyte, the PSSE

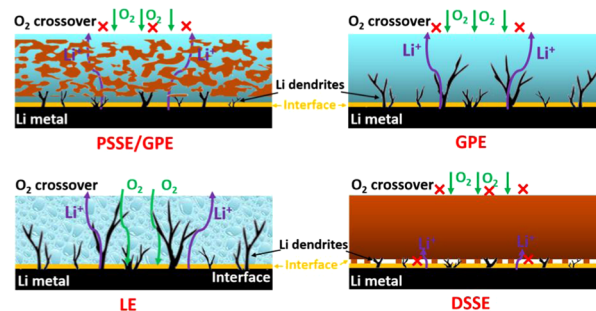


Figure 6. Schematic comparison of the effects of various electrolytes in Li–O₂ batteries.

backbone is flooded with GPE, presenting GPE features on the outer surface to ensure good contact with electrodes. The GPE buffer layers effectively decrease the interface resistance.^{50,51} As the porous backbone is infused with GPE, both the continuous GPE and the interconnected PSSE structure are Li-ion-conductive, delivering an overall high ionic conductivity. Moreover, the combination of the GPE filling and dense GPE layer on the outer surface can block the O₂ crossover to the Li metal anode, avoiding the Li corrosion.^{52,53} In addition, considering compatibility with the Li metal anode, the PSSE backbone acted as the rigid component to mechanically suppress Li dendrite growths. By contrast, the single-component electrolytes experience individual shortcomings. For instance, pure GPE has poor mechanical strength that cannot suppress Li dendrites.^{54–56} LE can neither suppress Li dendrites nor block O₂ crossover. Furthermore, the problematic LE can easily evaporate and leak.^{57,58} The rigid property of DSSE leads to interfacial contact issues with the electrodes.^{59,60} Although DSSE features good mechanical strength to be able to suppress Li dendrites, LLZTO-based electrolytes still suffer from the problem that Li dendrites go through the pellet along the grain boundary of electrolyte particles. The reason for the formation of Li dendrites in LLZTO pellet may be due to its high electronic conductivity and still some pores inside LLZTO pellet.⁶¹ Overall, the designed PSSE/GPE hybrid electrolyte possesses comprehensive advantages over other electrolytes for Li–O₂ battery.

CONCLUSIONS

In summary, we have successfully developed a PSSE/GPE hybrid solid electrolyte with gel polymer electrolyte infused in a 3D garnet microstructure for high-performance Li–O₂ batteries. The 3D garnet microstructure acted as a rigid component for mechanical support and Li dendrite suppression, while the continuous GPE in the 3D framework ensured a high ionic conductivity ($1.06 \times 10^{-3} \text{ S cm}^{-1}$) and overall compactness for blocking O₂ crossover. The flooded GPE on the outer surface of PSSE/GPE served as buffer layers for small interfacial resistance with electrodes. Benefiting from these combined merits, the Li metal symmetric cell with this hybrid electrolyte exhibited a significantly improved cycling stability (more than 6000 h, 250 days) with low overpotential; the demonstrating Li–O₂ battery delivered excellent cycling performance with a long cycling life of 194 cycles at a high cycling specific capacity of 1250 mA h g⁻¹. The present study reveals a novel class of hybrid solid electrolytes that offers an opportunity for advanced solid-state Li–O₂ batteries.

EXPERIMENTAL SECTION

Materials Synthesis. The pure GPE was prepared by a solution casting method. Typically, the mixed solution of PVDF-HFP polymer (0.6 g, M_w : 400 000), TEGDME solvent (1.6 g), and LiClO₄ salt (0.43 g) dissolved in acetone (20 mL) was prepared by vigorously stirring overnight. Then, the solution was cast in a poly(tetrafluoroethylene) (PTFE) dish and dried at room temperature for 3 days to remove acetone solvent, yielding the GPE. PSSE pellets were made by a template-assisted method. LLZTO (CAS Shanghai, China) powders (70 wt %) and PMMA templates (30 wt %) were mixed and ground with poly(vinyl butyral) (PVB) as the binder before pressed into pellets at 250 MPa. The as-obtained pellets were sintered at 450 °C for 2 h and followed by 1150 °C for 8 h. The DSSE pellets were made under the same conditions in the absence of PMMA templates. The hybrid electrolyte of PSSE/GPE was made by

immersing the PSSE pellet in the mixed solution for making GPE (with acetone). After drying, the PSSE/GPE was yielded.

Materials Characterization. The morphology, structure, and composition of the hybrid electrolyte and air electrode were characterized by SEM (Hitachi S-4800 and Hitachi S-3400), TEM (FEI TF30), Raman (HORIBA Scientific LabRAM HR), and X-ray diffraction (XRD) (D/Max-III-type, Cu K α X-ray source).

Electrochemical Measurements. The CNT–Mn₃O₄–RuO₂ air electrode was prepared as our previous report.⁴⁹ The as-made CNT–Mn₃O₄–RuO₂ was free-standing and used as the air electrode directly. The ionic conductivity of GPE and PSSE/GPE was evaluated by conducting the EIS test on the cell sandwiched with two stainless steel electrodes (Figure S5a). The ionic conductivity of DSSE electrolyte membrane (pellet) was evaluated by sputtering gold on both surfaces of LLZTO pellets as the current collector (Figure S5b). The PSSE/GPE hybrid electrolyte served as both electrolyte and separator in the solid-state Li metal symmetric cells and Li–O₂ batteries. All cells were assembled in an argon-filled glovebox (O₂ <0.1 ppm and H₂O <0.1 ppm). The electrochemical performance of Li–O₂ batteries was evaluated by assembling Swagelok-type cells and tested on the Arbin battery testing system in 1 atm O₂. The specific capacity of Li–O₂ batteries was calculated based on the mass of carbon. The EIS tests were performed on a Bio-Logic electrochemical workstation at open-circuit potential.

ASSOCIATED CONTENT

Supporting Information

The Supporting Information is available free of charge at <https://pubs.acs.org/doi/10.1021/acs.chemmater.0c03529>.

Digital photo, SEM images, schematic diagram, Nyquist plot, critical current density of PSSE/GPE, discharge/charge profiles, cycling stability, Raman spectra, and comparison of the cycling performance between this work and the works previously reported in the literature (PDF)

AUTHOR INFORMATION

Corresponding Author

Xueliang Sun – Department of Mechanical and Materials Engineering, University of Western Ontario, London, Ontario N6A 5B9, Canada; orcid.org/0000-0003-0374-1245; Email: xsun9@uwo.ca

Authors

Changtai Zhao – Department of Mechanical and Materials Engineering, University of Western Ontario, London, Ontario N6A 5B9, Canada

Qian Sun – Department of Mechanical and Materials Engineering, University of Western Ontario, London, Ontario N6A 5B9, Canada

Jing Luo – Department of Mechanical and Materials Engineering, University of Western Ontario, London, Ontario N6A 5B9, Canada

Jianneng Liang – Department of Mechanical and Materials Engineering, University of Western Ontario, London, Ontario N6A 5B9, Canada

Yulong Liu – Department of Mechanical and Materials Engineering, University of Western Ontario, London, Ontario N6A 5B9, Canada

Lei Zhang – Department of Mechanical and Materials Engineering, University of Western Ontario, London, Ontario N6A 5B9, Canada

Jiwei Wang – Department of Mechanical and Materials Engineering, University of Western Ontario, London, Ontario N6A 5B9, Canada

Sixu Deng – Department of Mechanical and Materials Engineering, University of Western Ontario, London, Ontario N6A 5B9, Canada

Xiaoting Lin – Department of Mechanical and Materials Engineering, University of Western Ontario, London, Ontario N6A 5B9, Canada

Xiaofei Yang – Department of Mechanical and Materials Engineering, University of Western Ontario, London, Ontario N6A 5B9, Canada

Huan Huang – Glabat Solid-State Battery Inc., London, Ontario N6G 4X8, Canada

Shangqian Zhao – China Automotive Battery Research Institute, Beijing 100088, P. R. China

Li Zhang – China Automotive Battery Research Institute, Beijing 100088, P. R. China

Shigang Lu – China Automotive Battery Research Institute, Beijing 100088, P. R. China

Complete contact information is available at:

<https://pubs.acs.org/10.1021/acs.chemmater.0c03529>

Funding

This work was supported by Natural Sciences and Engineering Research Council of Canada (NSERC), Canada Research Chair Program (CRC), China Automotive Battery Research Institute, Glabat Solid-State Battery Inc., Ontario Research Fund, Canada Foundation for Innovation (CFI), and Western University.

Notes

The authors declare no competing financial interest.

ACKNOWLEDGMENTS

All authors have given approval to the final version of the manuscript.

REFERENCES

- (1) Zhao, C.; Yu, C.; Li, S.; Guo, W.; Zhao, Y.; Dong, Q.; Lin, X.; Song, Z.; Tan, X.; Wang, C.; Zheng, M.; Sun, X.; Qiu, J. Ultrahigh-Capacity and Long-Life Lithium–Metal Batteries Enabled by Engineering Carbon Nanofiber–Stabilized Graphene Aerogel Film Host. *Small* **2018**, *14*, No. 1803310.
- (2) Lin, D.; Liu, Y.; Cui, Y. Reviving the lithium metal anode for high-energy batteries. *Nat. Nanotechnol.* **2017**, *12*, 194.
- (3) Cheng, X.-B.; Zhang, R.; Zhao, C.-Z.; Zhang, Q. Toward Safe Lithium Metal Anode in Rechargeable Batteries: A Review. *Chem. Rev.* **2017**, *117*, 10403–10473.
- (4) Zou, X.; Lu, Q.; Zhong, Y.; Liao, K.; Zhou, W.; Shao, Z. Flexible, Flame-Resistant, and Dendrite-Impermeable Gel-Polymer Electrolyte for Li–O₂/Air Batteries Workable Under Hurdle Conditions. *Small* **2018**, *14*, No. 1801798.
- (5) Lu, J.; Li, L.; Park, J.-B.; Sun, Y.-K.; Wu, F.; Amine, K. Aprotic and Aqueous Li–O₂ Batteries. *Chem. Rev.* **2014**, *114*, 5611–5640.
- (6) Zhang, Y.; Wang, L.; Guo, Z.; Xu, Y.; Wang, Y.; Peng, H. High-Performance Lithium–Air Battery with a Coaxial-Fiber Architecture. *Angew. Chem., Int. Ed.* **2016**, *55*, 4487–4491.
- (7) Zhao, C.; Yu, C.; Liu, S.; Yang, J.; Fan, X.; Huang, H.; Qiu, J. 3D Porous N-Doped Graphene Frameworks Made of Interconnected Nanocages for Ultrahigh-Rate and Long-Life Li–O₂ Batteries. *Adv. Funct. Mater.* **2015**, *25*, 6913–6920.
- (8) Yi, J.; Guo, S.; He, P.; Zhou, H. Status and prospects of polymer electrolytes for solid-state Li–O₂ (air) batteries. *Energy Environ. Sci.* **2017**, *10*, 860–884.
- (9) Liao, K.; Wu, S.; Mu, X.; Lu, Q.; Han, M.; He, P.; Shao, Z.; Zhou, H. Developing a “Water-Defendable” and “Dendrite-Free” Lithium–Metal Anode Using a Simple and Promising GeCl₄ Pretreatment Method. *Adv. Mater.* **2018**, *30*, No. 1705711.

- (10) Huang, Z.; Ren, J.; Zhang, W.; Xie, M.; Li, Y.; Sun, D.; Shen, Y.; Huang, Y. Protecting the Li-Metal Anode in a Li–O₂ Battery by using Boric Acid as an SEI-Forming Additive. *Adv. Mater.* **2018**, *30*, No. 1803270.

- (11) Liu, Y.; He, P.; Zhou, H. Rechargeable Solid-State Li–Air and Li–S Batteries: Materials, Construction, and Challenges. *Adv. Energy Mater.* **2018**, *8*, No. 1701602.

- (12) Yang, C.; Zhang, L.; Liu, B.; Xu, S.; Hamann, T.; McOwen, D.; Dai, J.; Luo, W.; Gong, Y.; Wachsman, E. D.; Hu, L. Continuous plating/stripping behavior of solid-state lithium metal anode in a 3D ion-conductive framework. *Proc. Natl. Acad. Sci. U.S.A.* **2018**, *115*, 3770–3775.

- (13) Zhang, H.; Liao, X.; Guan, Y.; Xiang, Y.; Li, M.; Zhang, W.; Zhu, X.; Ming, H.; Lu, L.; Qiu, J.; Huang, Y.; Cao, G.; Yang, Y.; Mai, L.; Zhao, Y.; Zhang, H. Lithiophilic-lithiophobic gradient interfacial layer for a highly stable lithium metal anode. *Nat. Commun.* **2018**, *9*, No. 3729.

- (14) Duan, H.; Yin, Y.-X.; Shi, Y.; Wang, P.-F.; Zhang, X.-D.; Yang, C.-P.; Shi, J.-L.; Wen, R.; Guo, Y.-G.; Wan, L.-J. Dendrite-Free Li-Metal Battery Enabled by a Thin Asymmetric Solid Electrolyte with Engineered Layers. *J. Am. Chem. Soc.* **2018**, *140*, 82–85.

- (15) Ding, F.; Xu, W.; Graff, G. L.; Zhang, J.; Sushko, M. L.; Chen, X.; Shao, Y.; Engelhard, M. H.; Nie, Z.; Xiao, J.; Liu, X.; Sushko, P. V.; Liu, J.; Zhang, J.-G. Dendrite-Free Lithium Deposition via Self-Healing Electrostatic Shield Mechanism. *J. Am. Chem. Soc.* **2013**, *135*, 4450–4456.

- (16) Pang, Q.; Liang, X.; Shyamsunder, A.; Nazar, L. F. An In Vivo Formed Solid Electrolyte Surface Layer Enables Stable Plating of Li Metal. *Joule* **2017**, *1*, 871–886.

- (17) Wang, A.; Zhang, X.; Yang, Y.-W.; Huang, J.; Liu, X.; Luo, J. Horizontal Centripetal Plating in the Patterned Voids of Li/Graphene Composites for Stable Lithium–Metal Anodes. *Chem* **2018**, *4*, 2192–2200.

- (18) Zhang, R.; Li, N.-W.; Cheng, X.-B.; Yin, Y.-X.; Zhang, Q.; Guo, Y.-G. Advanced Micro/Nanostructures for Lithium Metal Anodes. *Adv. Sci.* **2017**, *4*, No. 1600445.

- (19) Zhao, H.; Lei, D.; He, Y.-B.; Yuan, Y.; Yun, Q.; Ni, B.; Lv, W.; Li, B.; Yang, Q.-H.; Kang, F.; Lu, J. Compact 3D Copper with Uniform Porous Structure Derived by Electrochemical Dealloying as Dendrite-Free Lithium Metal Anode Current Collector. *Adv. Energy Mater.* **2018**, *8*, No. 1800266.

- (20) Kitaura, H.; Zhou, H. All-solid-state lithium-oxygen battery with high safety in wide ambient temperature range. *Sci. Rep.* **2015**, *5*, No. 13271.

- (21) Elia, G. A.; Hassoun, J. A Polymer Lithium–Oxygen Battery. *Sci. Rep.* **2015**, *5*, No. 12307.

- (22) Li, Y.; Wang, X.; Dong, S.; Chen, X.; Cui, G. Recent Advances in Non-Aqueous Electrolyte for Rechargeable Li–O₂ Batteries. *Adv. Energy Mater.* **2016**, *6*, No. 1600751.

- (23) Cheng, X.; Pan, J.; Zhao, Y.; Liao, M.; Peng, H. Gel Polymer Electrolytes for Electrochemical Energy Storage. *Adv. Energy Mater.* **2018**, *8*, No. 1702184.

- (24) Sun, J.; Zhao, N.; Li, Y.; Guo, X.; Feng, X.; Liu, X.; Liu, Z.; Cui, G.; Zheng, H.; Gu, L.; Li, H. A Rechargeable Li–Air Fuel Cell Battery Based on Garnet Solid Electrolytes. *Sci. Rep.* **2017**, *7*, No. 41217.

- (25) Bonnet-Mercier, N.; Wong, R. A.; Thomas, M. L.; Dutta, A.; Yamanaka, K.; Yogi, C.; Ohta, T.; Byon, H. R. A structured three-dimensional polymer electrolyte with enlarged active reaction zone for Li–O₂ batteries. *Sci. Rep.* **2015**, *4*, No. 7127.

- (26) Zhu, X. B.; Zhao, T. S.; Wei, Z. H.; Tan, P.; Zhao, G. A novel solid-state Li–O₂ battery with an integrated electrolyte and cathode structure. *Energy Environ. Sci.* **2015**, *8*, 2782–2790.

- (27) Wang, X.; Zhu, D.; Song, M.; Cai, S.; Zhang, L.; Chen, Y. A Li–O₂/Air Battery Using an Inorganic Solid-State Air Cathode. *ACS Appl. Mater. Interfaces* **2014**, *6*, 11204–11210.

- (28) Balaish, M.; Peled, E.; Golodnitsky, D.; Ein-Eli, Y. Liquid-Free Lithium–Oxygen Batteries. *Angew. Chem.* **2015**, *127*, 446–450.

- (29) Hassoun, J.; Croce, F.; Armand, M.; Scrosati, B. Investigation of the O₂ Electrochemistry in a Polymer Electrolyte Solid-State Cell. *Angew. Chem., Int. Ed.* **2011**, *50*, 2999–3002.
- (30) Gao, Z.; Sun, H.; Fu, L.; Ye, F.; Zhang, Y.; Luo, W.; Huang, Y. Promises, Challenges, and Recent Progress of Inorganic Solid-State Electrolytes for All-Solid-State Lithium Batteries. *Adv. Mater.* **2018**, *30*, No. 1705702.
- (31) Yu, X.; Manthiram, A. Electrode–Electrolyte Interfaces in Lithium–Sulfur Batteries with Liquid or Inorganic Solid Electrolytes. *Acc. Chem. Res.* **2017**, *50*, 2653–2660.
- (32) Zhu, X.; Zhao, T.; Tan, P.; Wei, Z.; Wu, M. A high-performance solid-state lithium–oxygen battery with a ceramic–carbon nanostructured electrode. *Nano Energy* **2016**, *26*, 565–576.
- (33) Liu, Y.; Li, B.; Cheng, Z.; Li, C.; Zhang, X.; Guo, S.; He, P.; Zhou, H. Intensive investigation on all-solid-state Li–air batteries with cathode catalysts of single-walled carbon nanotube/RuO₂. *J. Power Sources* **2018**, *395*, 439–443.
- (34) Bae, J.; Li, Y.; Zhang, J.; Zhou, X.; Zhao, F.; Shi, Y.; Goodenough, J. B.; Yu, G. A 3D Nanostructured Hydrogel-Framework-Derived High-Performance Composite Polymer Lithium-Ion Electrolyte. *Angew. Chem., Int. Ed.* **2018**, *57*, 2096–2100.
- (35) Zhu, X. B.; Zhao, T. S.; Wei, Z. H.; Tan, P.; An, L. A high-rate and long cycle life solid-state lithium–air battery. *Energy Environ. Sci.* **2015**, *8*, 3745–3754.
- (36) Fu, K.; Gong, Y.; Hitz, G. T.; McOwen, D. W.; Li, Y.; Xu, S.; Wen, Y.; Zhang, L.; Wang, C.; Pastel, G.; Dai, J.; Liu, B.; Xie, H.; Yao, Y.; Wachsman, E. D.; Hu, L. Three-dimensional bilayer garnet solid electrolyte based high energy density lithium metal–sulfur batteries. *Energy Environ. Sci.* **2017**, *10*, 1568–1575.
- (37) Yang, C.; Xie, H.; Ping, W.; Fu, K.; Liu, B.; Rao, J.; Dai, J.; Wang, C.; Pastel, G.; Hu, L. An Electron/Ion Dual-Conductive Alloy Framework for High-Rate and High-Capacity Solid-State Lithium-Metal Batteries. *Adv. Mater.* **2019**, *31*, No. 1804815.
- (38) Zhao, C.-Z.; Zhang, X.-Q.; Cheng, X.-B.; Zhang, R.; Xu, R.; Chen, P.-Y.; Peng, H.-J.; Huang, J.-Q.; Zhang, Q. An anion-immobilized composite electrolyte for dendrite-free lithium metal anodes. *Proc. Natl. Acad. Sci. U.S.A.* **2017**, *114*, 11069–11074.
- (39) Bae, J.; Li, Y.; Zhao, F.; Zhou, X.; Ding, Y.; Yu, G. Designing 3D nanostructured garnet frameworks for enhancing ionic conductivity and flexibility in composite polymer electrolytes for lithium batteries. *Energy Storage Mater.* **2018**, *15*, 46–52.
- (40) Han, X.; Gong, Y.; Fu, K.; He, X.; Hitz, G. T.; Dai, J.; Pearce, A.; Liu, B.; Wang, H.; Rubloff, G.; Mo, Y.; Thangadurai, V.; Wachsman, E. D.; Hu, L. Negating interfacial impedance in garnet-based solid-state Li metal batteries. *Nat. Mater.* **2017**, *16*, 572.
- (41) Chi, S.-S.; Liu, Y.; Zhao, N.; Guo, X.; Nan, C.-W.; Fan, L.-Z. Solid polymer electrolyte soft interface layer with 3D lithium anode for all-solid-state lithium batteries. *Energy Storage Mater.* **2019**, *17*, 309–316.
- (42) Yu, C.; Zhao, C.; Liu, S.; Fan, X.; Yang, J.; Zhang, M.; Qiu, J. Polystyrene sphere-mediated ultrathin graphene sheet-assembled frameworks for high-power density Li–O₂ batteries. *Chem. Commun.* **2015**, *51*, 13233–13236.
- (43) Liu, Q.-C.; Liu, T.; Liu, D.-P.; Li, Z.-J.; Zhang, X.-B.; Zhang, Y. A Flexible and Wearable Lithium–Oxygen Battery with Record Energy Density achieved by the Interlaced Architecture inspired by Bamboo Slips. *Adv. Mater.* **2016**, *28*, 8413–8418.
- (44) Yang, X.-Y.; Xu, J.-J.; Chang, Z.-W.; Bao, D.; Yin, Y.-B.; Liu, T.; Yan, J.-M.; Liu, D.-P.; Zhang, Y.; Zhang, X.-B. Blood-Capillary-Inspired, Free-Standing, Flexible, and Low-Cost Super-Hydrophobic N-CNTs@SS Cathodes for High-Capacity, High-Rate, and Stable Li–Air Batteries. *Adv. Energy Mater.* **2018**, *8*, No. 1702242.
- (45) Tikekar, M. D.; Choudhury, S.; Tu, Z.; Archer, L. A. Design principles for electrolytes and interfaces for stable lithium–metal batteries. *Nat. Energy* **2016**, *1*, No. 16114.
- (46) Xu, L.; Tang, S.; Cheng, Y.; Wang, K.; Liang, J.; Liu, C.; Cao, Y.-C.; Wei, F.; Mai, L. Interfaces in Solid-State Lithium Batteries. *Joule* **2018**, *2*, 1991–2015.
- (47) Yu, X.; Manthiram, A. Electrode–electrolyte interfaces in lithium-based batteries. *Energy Environ. Sci.* **2018**, *11*, 527–543.
- (48) Zhang, Z.; Shao, Y.; Lotsch, B.; Hu, Y.-S.; Li, H.; Janeck, J.; Nazar, L. F.; Nan, C.-W.; Maier, J.; Armand, M.; Chen, L. New horizons for inorganic solid state ion conductors. *Energy Environ. Sci.* **2018**, *11*, 1945–1976.
- (49) Zhao, C.; Yu, C.; Banis, M. N.; Sun, Q.; Zhang, M.; Li, X.; Liu, Y.; Zhao, Y.; Huang, H.; Li, S.; Han, X.; Xiao, B.; Song, Z.; Li, R.; Qiu, J.; Sun, X. Decoupling atomic-layer-deposition ultrafine RuO₂ for high-efficiency and ultralong-life Li–O₂ batteries. *Nano Energy* **2017**, *34*, 399–407.
- (50) Luo, W.-B.; Chou, S.-L.; Wang, J.-Z.; Kang, Y.-M.; Zhai, Y.-C.; Liu, H.-K. A hybrid gel–solid-state polymer electrolyte for long-life lithium oxygen batteries. *Chem. Commun.* **2015**, *51*, 8269–8272.
- (51) Luo, W.; Gong, Y.; Zhu, Y.; Li, Y.; Yao, Y.; Zhang, Y.; Fu, K.; Pastel, G.; Lin, C.-F.; Mo, Y.; Wachsman, E. D.; Hu, L. Reducing Interfacial Resistance between Garnet-Structured Solid-State Electrolyte and Li-Metal Anode by a Germanium Layer. *Adv. Mater.* **2017**, *29*, No. 1606042.
- (52) Jung, K.-N.; Lee, J.-I.; Jung, J.-H.; Shin, K.-H.; Lee, J.-W. A quasi-solid-state rechargeable lithium–oxygen battery based on a gel polymer electrolyte with an ionic liquid. *Chem. Commun.* **2014**, *50*, 5458–5461.
- (53) Guo, Z.; Li, C.; Liu, J.; Wang, Y.; Xia, Y. A Long-Life Lithium–Air Battery in Ambient Air with a Polymer Electrolyte Containing a Redox Mediator. *Angew. Chem., Int. Ed.* **2017**, *56*, 7505–7509.
- (54) Zhao, C.; Liang, J.; Sun, Q.; Luo, J.; Liu, Y.; Lin, X.; Zhao, Y.; Yadegari, H.; Banis, M. N.; Li, R.; Huang, H.; Zhang, L.; Yang, R.; Lu, S.; Sun, X. Ultralong-Life Quasi-Solid-State Li–O₂ Batteries Enabled by Coupling Advanced Air Electrode Design with Li Metal Anode Protection. *Small Methods* **2018**, *3*, No. 1800437.
- (55) Tu, Z.; Yu, K.; Lu, Y.; Archer, L. A. Nanoporous Polymer–Ceramic Composite Electrolytes for Lithium Metal Batteries. *Adv. Energy Mater.* **2014**, *4*, No. 1300654.
- (56) Wu, S.; Yi, J.; Zhu, K.; Bai, S.; Liu, Y.; Qiao, Y.; Ishida, M.; Zhou, H. A Super-Hydrophobic Quasi-Solid Electrolyte for Li–O₂ Battery with Improved Safety and Cycle Life in Humid Atmosphere. *Adv. Energy Mater.* **2017**, *7*, No. 1601759.
- (57) Manthiram, A.; Yu, X.; Wang, S. Lithium battery chemistries enabled by solid-state electrolytes. *Nat. Rev. Mater.* **2017**, *2*, No. 16103.
- (58) Chen, W.; Yin, W.; Shen, Y.; Huang, Z.; Li, X.; Wang, F.; Zhang, W.; Deng, Z.; Zhang, Z.; Huang, Y. High areal capacity, long cycle life Li–O₂ cathode based on highly elastic gel granules. *Nano Energy* **2018**, *47*, 353–360.
- (59) Zhang, X.-P.; Wen, Z.-Y.; Zhang, T. Ionic activation via a hybrid IL–SSE interfacial layer for Li–O₂ batteries with 99.5% coulombic efficiency. *J. Mater. Chem. A* **2018**, *6*, 12945–12949.
- (60) Wu, B.; Wang, S.; Evans Iv, W. J.; Deng, D. Z.; Yang, J.; Xiao, J. Interfacial behaviours between lithium ion conductors and electrode materials in various battery systems. *J. Mater. Chem. A* **2016**, *4*, 15266–15280.
- (61) Han, F.; Westover, A. S.; Yue, J.; Fan, X.; Wang, F.; Chi, M.; Leonard, D. N.; Dudney, N. J.; Wang, H.; Wang, C. High electronic conductivity as the origin of lithium dendrite formation within solid electrolytes. *Nat. Energy* **2019**, *4*, 187–196.